# A 2D MODEL TO DESIGN MHD INDUCTION PUMPS

*R. Stieglitz, J. Zeininger*

*Institute for Nuclear and Energy Technologies (IKET), Forschungszentrum Karlsruhe, Post Box 3640, D-76021 Karlsruhe, Germany*

**1. Introduction.** Technical liquid metal systems accompanied by a thermal transfer of energy such as reactor systems, metallurgical processes, metal refinement, casting etc. require a forced convection of the fluid. The elevated temperatures and more often the environmental conditions as e.g. in a nuclear environment pumping principles are required, in which rotating parts are absent. Additionally, in many applications a controlled atmosphere is indispensable, in order to ensure the structural integrity of the duct walls. An interesting option to overcome the sealing problem of a mechanical pump towards the ambient is offered by induction systems. Although their efficiency is compared to the one of turbo machines quite low they service several advantages, which are attractive to the specific requirements in liquid metal applications such as:

- low maintenance costs due to absence of sealings, bearings and moving parts;
- low degradation rate of the structural material;
- simple replacement of the inductor without cut of the piping system;
- fine regulation of flow rate by different inductor connections;
- change of pump characteristics without change of the mechanical set-up.

Within article general design requirements of electro-magnetic pumps (EMPS) are elaborated. The design of two annular linear induction pumps operated with sodium and lead bismuth are presented and the calculated pump characteristics and experimentally obtained data are compared. In this context physical effects leading to deviations between the model and the real data are addressed. Finally, the main results are summarized.

**2. Design equations for linear induction pumps.** The operation principle of magneto-hydrodynamic induction pumps is similar to that of an asynchronous motor. In order that the magnetic field can induce an electric current within the fluid it must change in time. Since the resulting Lorentz-force should have a defined direction a travelling magnetic field has to be applied to the fluid. A three phase AC motor utilizes a rotating magnetic field, which is excited by an electric current in the stator. The inductor of an electro-magnetic pump is also composed like a stator of an AC motor, if one considers the stator to be cut and expanded into a plane. In an AC motor the magnetic field, which is generated by the electric current and amplified by the ferromagnetic iron sheets, travels along the $z$-axis in an idealized imagination as a sinusoidal wave. It 'runs' along this axis with the so-called synchronous velocity $v_B$. In reality, however, the magnetic field distribution 'runs', because the stator or inductor is fed by an AC current. The three distributions given by the three phase current merge and create a quasi-sinusoidal shape of the magnetic field distribution. The synchronous velocity $v_B$ is calculated as the product of the wave length $\lambda$ of the magnetic induction and the AC supply frequency $f$. The wavelength $\lambda$g defined as the distance between two adjacent peaks of the magnetic induction is an essential geometric parameter of the inductor and can be conceived as the actual distance between the north and

the south poles of the magnetic field. This travelling magnetic field induces an electric current $j$ within the fluid, which is also of quasi sinusoidal shape and also travelling. The interaction of the magnetic induction $B$ and the induced current $j$ results in a Lorentz force, which pulls the fluid in direction of the induction. The fluid velocity $v_f$ is always smaller than that of the magnetic field $v_B$. If they would be identical no induction takes place and thus no electric current and force establishes. The same holds for asynchronous motors, in which the angular velocity of the rotor is always a little smaller than that of the rotating stator field. (If the fluid velocity would be larger than the speed of the field the device would act as a generator.) The difference between both velocities additionally divided by the synchronous velocity $v_B$ is called the slip $s$. with $s = (v_B - v_f)/v_B$.

*2.1. Ideal linear induction pump.* Consider an element of the dimensions $dx$, $dy$ and $dz$ as shown in fig. 1, where the current density is $j_y$ and the induction is $H_x$. Equating forces acting on such an element in $z$-direction, we obtain a balance between Lorentz ($j_y \quad H_x$) and pressure forces, which is given by eq. 1a. The total pressure difference $p_z$ developed in a pump of the effective length $L$ is then given by eq. 1b.; and if the pressure is uniform across the tube in the $x$- and $y$ the gross output power $P_0$ is given by eq. 1c.

$$\frac{\partial p}{\partial z} = j_y H_x,\ p_z = \int_{z=0}^{z=L} j_y H_x\, dz\,,\ P_0 = p_z \cdot (v \cdot a \cdot b) \tag{1}$$

where $a$ and $b$ are the duct dimensions according to fig. 1, $v$ the mean velocity and $p$ the pressure. The ohmic loss $P_{Ohm}$ in the fluid, again assuming uniformity, is

$$P_{Ohm} = \frac{(a \cdot b)}{\sigma} \int_{z=0}^{z=L} j_y^2\, dz, \tag{2}$$

where $\sigma$ is the specific electric conductivity of the fluid in $A/(Vm)$. These expressions are basic to all forms of EMPs. Other losses are the hydraulic friction loss $P_{hydr}$, the winding loss $P_W$, losses in the tube walls $P_{tube}$, eddy current losses at in- outlet, core losses etc.. In addition, there can be another substantial losses.

Fig. 1: Sketch of a linear induction pump and coordinate system.

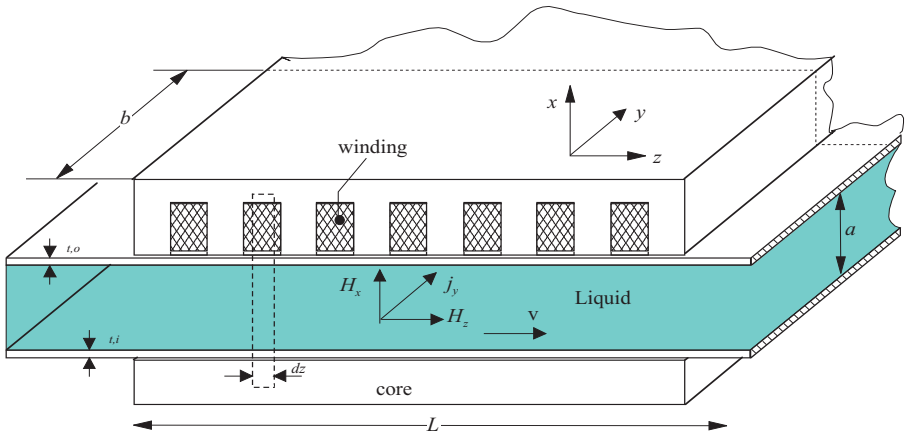


The design equations for the ideal forms of annular inductions pumps will be considered together by assuming the pump to be flat and of infinite width in $y$-direction $a/b << 1$. A strip of finite width $b$of this infinite extent corresponds to the

mean circumference $d_m$ of the annular gap in the ALIP. Only the $x-$component of $H$ and the $y-$component of the current $j$ will be assumed here to exist. The relation between the current density in the fluid $j_f$, in the tube walls $j_t$ the field $H$, the core flux $\Phi$ per unit length, the magnetizing ampere-turns $\partial NI_m/\partial z$ and the induced voltage per turn $\phi_i/N$ can be derived. Since flux lines are continuous one can write eq. 3a and Faradays law yields eq. 3b.

$$\Phi_Z - \Phi_0 = \int_0^z b\, H\, dz \text{ or } H = \frac{1}{b}\,\frac{\partial \Phi}{\partial z},\ \frac{10^8 b}{\sigma} j_f = -\frac{d\Phi}{dt} = -\left(\frac{\partial \Phi}{\partial t} + v\,\frac{\partial \Phi}{\partial z}\right) \quad (3)$$

The electric current density in the tube walls $j_t$ is derived from $j_f$ by replacing $\sigma$ with $\sigma_t$ and setting $v = 0$. Applying Amperes law to the circuit of width $dz$ one obtains equation 4

$$\frac{\partial N\ I_m}{\partial z} = -\frac{10\,a}{4\,\pi}\,\frac{\partial H}{\partial z} = -\frac{10\,a}{4\,\pi\,b}\,\frac{\partial^2 \Phi}{\partial z^2}\ . \quad (4)$$

The voltage per turn induced $\phi_i$ in the winding is given by eq. 5a and if the flux is assumed to be of the form $\Phi = \Phi_0\ cos(\omega\ \ t - \psi)$, as in the induction motor, where $\psi$=$2\pi z/\lambda$, then one obtains eq.5b. Here, $H_P$ is the peak induction.

$$\frac{\phi_i}{N} = \frac{1}{10^8}\,\frac{\partial \Phi}{\partial t}\ ; \quad H = H_P \sin(\omega\, t - \psi) \text{ with } H_P = \left(\frac{2\pi}{\lambda\, b}\right)\,\Phi \quad (5)$$

Similarly using equations 3-5 expressions for $j_f$ , $j_t$ $\partial NI_m/\partial z$ and $\phi_i/N$ can be derived.

$$\begin{array}{cc} j_f = \frac{\sigma\, s\, v_B}{10^8}\ H_P \sin(\omega\, t - \psi)\,; & \frac{\partial NI_m}{\partial z} = \frac{5\,a}{\lambda}\ H_P \cos(\omega\, t - \psi)\,; \\ j_t = \frac{\sigma_t\ v_B}{10^8}\ H_P \sin(\omega\, t - \psi)\ ; & \frac{\phi_i}{N} = \frac{v_B\, b}{10^8}\ H_P \sin(\omega\, t - \psi) \end{array} \quad (6)$$

If these are substituted into eq. 1 and 2 expressions can be deduced for the pump pressure $p$, the gross power output $P_0$, and the ohmic losses $P_{Ohm}$ in the fluid and the tube wall $P_{tube}$. For $P_0$ and $P_{Ohm}$ the results are:

$$P_0 = P_\lambda\ s\ (1-s) \text{ and } P_{Ohm}\ = P_\lambda\ s^2 \text{ where } P_\lambda = \frac{v_B^2}{2\,\cdot 10^{16}}\,a\,b\,\sigma\,\lambda\,H_p^2. \quad (7)$$

An immediate result of the calculation is the ideal efficiency $\eta_i$, which is defined by $\eta_i = P_0/(P_0 + P_{Ohm})$=$(1-s)$. The equations of the ideal case are of limited validity and in fact only apply to the mid-section of a linear induction pump.

*2.2. End effects in the linear induction pump.* It was assumed tacitly that the flux $\Phi$ is of the form $\Phi_0\ cos(\omega t - \psi)$ over the length $L$ of the pump, $0< z < L$, and the fact that it is zero everywhere outside these limits is ignored. If the effect of the discontinuities of the ends are now considered it is evident from equations 3a and 4 that infinities are produced in $H$ and $\partial NI_m/\partial z$ which are not possible to realize in practice. Therefore, assuming the other limiting condition that the magnetizing current distribution $\partial NI_m/\partial z$ is of $cos(\omega t - \psi)$ form over the length of the pump and is zero outside. For consistency say

$$\frac{\partial NI_m}{\partial z} = \frac{5\,d}{\lambda}\ H_P \cos(\omega\, t - \psi) \quad . \quad (8)$$

The field and flux can be obtained by integrating twice according to eqs. 3a and 5. If the boundary conditions are inserted, namely $\Phi_0 = \Phi_{2n\pi}$=0, then one obtains

$$H = H_P \sin(\omega\, t - \psi)\ ; \quad \Phi = \Phi_0\ [\cos(\omega\, t - \psi) - \cos(\omega\, t)]\ . \quad (9)$$

It will be seen that $H$ and $\partial NI_m/\partial z$ are as before but $\Phi$ is different, being supplemented by the pulsating term $cos(\omega \quad t)$. A repetition of the calculation of power output $P_0$, and ohmic losses $P_{Ohm}$ and efficiency $\eta_i$ yields eqs. 10a-c:

$$\begin{gathered} P_0 = P_\lambda\, s\, (1-s)\ ;\ P_{Ohm}\ = P_\lambda\ \left(1+s^2\right)\ ; \\ \eta_i = (1-s)\ \cdot \left(\tfrac{s}{1+s}\right) \text{ again with } P_\lambda = \tfrac{v_B^2}{2\cdot 10^{16}}\, a\, b\, \sigma\, \lambda\, H_p^2. \end{gathered} \tag{10}$$

Comparing eqs. 7 with 10 shows that the effect of the pulsating component of the flux is to add a pulsating component of the current in the liquid metal, which performs no useful work but increases the ohmic losses by a factor $(1+s^2)/s^2$ and lowers the efficiency by a factor $s/(1+s)$. For example, at a slip of 50%, where the maximum power can be achieved, the ideal efficiency is lowered from 50% to 16.7%. It is evident that these effects are much too large to be tolerated in power conversion systems. A dramatic optimisation of the pump performance could be realized if the windings at the in and outlet are graded, in order to get a smoother magnetic flux distribution and thus smaller leakage currents. A much simpler way to reduce the end losses is to grade the winding over the end sections and leave the mid region uniform. This yields a simpler arrangement, see Stieglitz (2003).

*2.3. Winding design.* The total current in the winding includes the magnetizing component $\partial NI_m/\partial z$ and components which cancel the magnetic effects of the current in the liquid and the tube walls by transformer action. The liquid metal current component is $\partial NI_m/\partial z$ =-$j_f a$and the tube wall current component is given by $-(k_{t1}/s)j_f a$. Thus, the ideal distribution of winding current is the vector sum

$$\frac{\partial NI_T}{\partial z} = \frac{\partial NI_M}{\partial z} + \frac{\partial NI_f}{\partial z}\left(1+\frac{k_{t1}}{s}\right). \tag{11}$$

For a three phase winding with $m$ coils per phase and per pole and one coil per slot the total coil current-turns at the position $z$ are

$$NI_T = \frac{\pi}{3}\int_{z-\lambda/12m}^{z+\lambda/12m} \frac{\partial NI_T}{\partial z} \quad dz. \tag{12}$$

The factor $\pi$ /3 is inserted to give agreement with the analysis of a 3-phase winding and would tend to unity as the number of phases is increased. For the mid section coils equation 12 can be written as eq. 13a., in which $k_d$ has the same form as the winding distribution factor that is $k_d$ =$(1/2m)$ sin$(30^\circ/m)$. The voltage per turn required to excite the coil is obtained by eq. 13b.

$$NI_T = \frac{\lambda}{6\, m\, k_d}\left(\frac{\partial NI_T}{\partial z}\right), \quad \frac{\phi}{N} = \left(\frac{\partial \Phi}{\partial t}\right)_z + (NI_T)_z\left(\frac{Z}{N^2}\right), \tag{13}$$

where $Z$ is the coil impedance (leakage reactance and resistance) calculated as in other electrical machines. The eqs. 11, 12 and 13b can be applied when designing the coils for both mid and end sections. A calculation of the coil Ampere-turns by the method of eq.12 is unorthodox but is suggested since it works equally to end and mid section coils.

*2.4. Flux penetration in the induction pump.* It is often desirable to employ a large channel width $a$ in a large pump, but it leads to a large value of $a/\lambda$, since $\lambda$ increases only little as the size of the pump is increased. This is because the slip $s$ tends to decrease with size, and although the permissible fluid velocity $v_f$ increases, the synchronous velocity $v_B$ = $v_f$/(1-$s$) remains virtually unchanged.

Thus, if the frequency is constant $\lambda = v_B/f$ is also virtually independent of the pump size. The use of a large $a/\lambda$ is liable to create difficulties due to the limited flux penetration in the gap. So it is necessary to examine these effects.

So far, it has been assumed that the field crosses the gap perpendicularly so that the $H_y-$ and $H_z$–components are absent. The assumption that $H_y$ is zero is reasonable but it is inappropriate to assume $H_z$ is zero; this is equivalent to ignoring flux penetration effects or, on other words, the reactive impedance to current flow in the liquid metal. A more accurate picture of the field in the gap shows $H_x$ increasing as the winding is approached, and $H_x$ also increasing from zero at the core to an appreciable value on the winding side of the gap. The field variation within the liquid alters the pressure distribution, making $p_z$ low on the core side and also introducing a component $p_x$, due to the interaction of $j_y$ and $H_z$. This in turn makes the fluid velocity $v_z$ vary across the gap and introduces a $v_x$–component. An exact calculation of these effects is complicated for a laminar flow and it is impossible for turbulent flows, which appear mostly in EMPs, because magnetohydrodynamic effects modify the turbulence structure and thus an isotropic turbulent diffusivity can not be assumed. Nevertheless, useful results can be obtained assuming the $H_z$–component of the field to be present in addition to the $H_x$–component, the velocity uniform of value $v_f$ and the $v_x$–component to be absent. Assume, therefore, that the liquid velocity $v_f$ is constant, and that the components of $H$ and $j$ exist in the following form:

$$H_x = H_1(x)\ \exp\left[i\omega\left(t-\frac{z}{v_B}\right)\right]\ ;\quad H_z = H_2(x)\ \exp\left[i\omega\left(t-\frac{z}{v_B}\right)\right]\ ; j_y = J(x)\ \exp\left[i\omega\left(t-\frac{z}{v_B}\right)\right]\ . \tag{14}$$

Under these conditions Maxwells first and second eqs. may be written as eqs 15a-c.

$$\frac{\partial H_x}{\partial z} - \frac{\partial H_z}{\partial x} = \frac{4\pi}{10} j_y ; \frac{10^8}{\sigma}\ \frac{\partial j_y}{\partial z} = -\ \frac{\partial H_x}{\partial t} - v_f \frac{\partial H_x}{\partial z}\ ; \frac{10^8}{\sigma}\ \frac{\partial j_y}{\partial x} = -\ \frac{\partial H_z}{\partial t} - v_f \frac{\partial H_z}{\partial z}. \tag{15}$$

Substituting eqs. 14 into 15 and solving for $H_1$ and $H_2$ one obtains

$$\begin{gathered}\frac{\partial^2 H_1}{\partial x^2} = \gamma^2 H_1\ ,\ \frac{\partial^2 H_2}{\partial x^2} = \gamma^2 H_2\ ,\ \frac{\partial H_1}{\partial x} = \frac{2\pi i}{\lambda}\ H_2, j = \frac{\sigma\, s\, v_B}{10^8}\ H_1 \\ \text{with } \gamma = \frac{2\pi}{\lambda}\sqrt{1+i\,h} \quad \text{and } h = \frac{2}{10^9}\,\sigma\, s\,\lambda\, v_B \quad .\end{gathered} \tag{16}$$

The boundary conditions which must be satisfied are $H_2$ =0 and from 16c, d

$$\frac{dH_1}{dx} = 0 \text{ at } x = 0 \quad . \tag{17}$$

This assumes that the core is of infinite permeability and cannot sustain the field $H_2$ parallel to its surface. For the second boundary condition many forms are possible. If the winding current is known, on can write

$H_2 = H_{2a}$ and $\frac{dH_1}{\partial x} = \frac{2\pi i}{\lambda}\ H_{2a}$ at $x = a$ ,with $H_{2a} = \left(\frac{4\pi}{10}\right)\ \frac{dNI_T}{dz}$ . (17b, c)

The latter expression is a reasonable approximation in most cases. If the supply voltage is known, or more accurately the induced voltage $\phi_i$ which is the supply voltage less the voltage drop in the winding impedance, then the following relation holds.

$$H_1 = H_a \text{ at } x = a \text{ where } \frac{\phi_i}{N} = \frac{v_B b\ i\ H_a}{10^8} \quad . \tag{18}$$

A further possibility is to suppose that the mean field across the gap is known

$$\frac{1}{a}\int_{x=0}^{x=a} H_1\, dx = H_p\ , \tag{19}$$

using the same symbol $H_P$ as before but denoting now the peak value in time of the mean gap field. Any of the eqs. 17-19 can be employed in solving eqs. 16; all have relative merits but eq. 19 appears to be most convenient when comparisons with previous expressions are to be made. This boundary condition will be employed together with the one of eq. 17. The analytic solution reduces then to

$$\frac{H_1}{H_P} = \quad \frac{\gamma\, a \quad \cosh(\gamma\, x)}{\sinh(\gamma\, a)}\,. \tag{20}$$

It is useful for design purposes to evaluate eq. 21, which yields the results of eq. 22.

$$\frac{H_a}{H_P} = \quad \frac{\gamma\, a}{\tanh(\gamma\, a)} = \left|\frac{H_a}{H_P}\right| \exp(i\,\varsigma)\,. \tag{21}$$

$$\left|\tfrac{H_a}{H_P}\right| = (\cosh M + \cos N_1)\ \sqrt{\tfrac{M^2+N_1^2}{(\sinh M)^2+(\sin N_1)^2}}\ ;\text{and } \varsigma = \tfrac{1}{\arctan\left(\frac{N_1}{M}\right)} - \tfrac{1}{\arctan\left(\frac{\sin N_1}{\sinh M}\right)}\ ;$$
$$\text{where } M = \tfrac{4\,\pi\,a}{\lambda}\ \sqrt{\tfrac{\sqrt{1+h^2}+1}{2}}\ \text{ and } N_1 = \tfrac{4\,\pi\,a}{\lambda}\ \sqrt{\tfrac{\sqrt{1+h^2}-1}{2}}. \tag{22}$$

It is also desirable to know the pressure difference on either side of the channel. This can be done by substituting eqs. 16c, d and eq. 20 into relation 1b. An integration leads to

$$\frac{p_a}{p_0} = \quad \frac{\cosh M + \cos N_1}{2}\,. \tag{23}$$

The gross power output $P_0$ based on a pressure averaged across the gap and in time as well as the ohmic loss in the fluid $P_{Ohm}$ are given by eqs. 24.

$$\begin{gathered} P_0 = P_\lambda\, s\,(1-s)\cdot\zeta \quad \text{and} \quad P_{Ohm} = P_\lambda\, s^2\ \cdot\zeta; \\ \text{with } P_\lambda = \tfrac{v_B^2}{2\cdot 10^{16}}\, a\, b\, \sigma\, \lambda\, H_p^2 \quad \text{and } \zeta = \tfrac{\left(M^2+N_1^2\right)\left(\frac{\sinh M}{M}+\frac{\sin N_1}{N_1}\right)}{4(\cosh M-\cos N_1)} \end{gathered} \tag{24}$$

*2.5. Final design equations.* In the previous sections the basic steps for the calculation of an EMP have been derived. With the given design parameters we now can calculate the operational parameters of the pump. Since the internal heating of the coil windings determines the achievable pressure head, the coils have to be designed in such a way that an optimal connection between the coils for a given pressure head leads to a minimum electrical current density. For an ideal ALIP (Annular Linear Induction Pump) having fine displaced coils, in which the slot width of the current carrying coils as smaller than the active pump length L, eq. 25 can be derived.

$$\frac{J^2}{\Delta p} = \frac{\left(\frac{2\pi\,a}{\mu_0 f \lambda^2}\right)^2 + \left(\delta_t\sigma_t + \left(1-\frac{v_f}{\lambda f}\right)\delta_f\sigma_f\right)^2}{\sigma_f L \frac{\left(1-\frac{v_f}{\lambda f}\right)}{\lambda f}} \tag{25}$$

Inserting the design parameters ( or geometrical extensions) into eq. 25 and postulating the required flow rate and pressure head $\Delta p$ one obtains the electric current to be supplied by windings to the duct as a function of the wavelength $\lambda$ at a given frequency $f$ of the travelling magnetic field. Using eq. 26 one can calculate the electric potential in the windings $\phi_i$ to obtain $\Delta p$

$$\frac{\phi_i^2}{\Delta p} = \quad \frac{(\pi d_m)^2\ \lambda\, f}{\sigma\, L\, \left(1-\frac{v_f}{\lambda f}\right)}\,. \tag{26}$$

The peak magnetic induction $H_P$ directly at the coils can then be calculated.

$$H_p = \quad \frac{\phi_i}{(\lambda\, f)\, \pi\; d_m}\; . \tag{27}$$

Finally, the peak magnetic field is amplified by packages of ferromagnetic sheets, which own a magnetic permeability $\mu$ being significantly larger than unity. In order to calculate the effective magnetic permeability leading to the amplification of the induction we have to integrate the room filling of the material in the active part (, which means the height of the windings, the inner core and the space in between which is the area to be pumped). The result has to be averaged over the whole volume being treated. Using this volume averaging procedure a mean magnetic permeability can be defined, which allows to treat the whole ferro-magnetic parts in the active part of the pump as one domain. The real current density $J_{real}$per wave length $\lambda$ is given by the geometrical design of the slots and the windings as well as the line current $I_L$ of the power supply, and can be calculated with eq. 28.

$$J_{real} = \frac{n_{\text{current turns}} \cdot n_{slots} \cdot I_L}{\lambda}\; . \tag{28}$$

*2.6. Power balance.* The electric power input in the system using a conventional 3-phase power supply with the potential $\phi$ and the current $I_L$ yields at the operation point of a pump to an electric gross power input given by eq. 29a, in which $\varphi$gs the phase shift between voltage and current. The total hydraulic pumping power is given by eq. 29b.

$$P_{Input} = \sqrt{3} \cdot \phi \cdot I_L \cdot \cos\varphi \; , P_{hydraulic} = \Delta p \cdot v_f \cdot \frac{\pi}{4} \left(d_a^2 - d_i^2\right) \tag{29}$$

In order to determine the hydraulic losses in the pump the hydraulic Reynolds number has to be calculated using eq. 30a, where $d_h$ is the hydraulic diameter ($d_h = d_a - d_i$) and $\nu$ the kinematic viscosity. The loss factor $\xi_F$ can be calculated using the Blasius relation given in eq. 30b.

$$Re = \frac{v_f \cdot d_h}{\nu}\; , \quad \xi_F = \frac{0.3164}{\sqrt[4]{Re}} \quad . \tag{30}$$

The pressure drop $\Delta p_{viscous}$ through the whole pumping duct can be obtained by eq. 31a. There, the hydraulic pressure drop coefficients $\xi_{i,o}$ are obtained using form relations collected in the book of Zierep& Bühler (1991). Knowing the pressure drop in the duct the power loss due to viscous forces $P_{viscous}$ can be easily evaluated using relation 31b.

$$\Delta p_{viscous} = \frac{\rho}{2} \cdot v_f^2 \cdot\; L\; \left(\xi_F + \xi_{i,o}\right)\; , \quad P_{viscous} = \Delta p_{viscous} \cdot v_f \cdot \frac{\pi}{4} \left(d_a^2 - d_i^2\right) \quad . \tag{31}$$

The ohmic losses $P_{ohm}$ within the fluid and the losses due pulsating component of the flux $P_\omega$ are:

$$P_{Ohm} = P_\lambda\; s^2 \quad , P_\omega = P_\lambda \frac{\left(1 + s^2\right)}{s^2} \quad , \tag{32}$$

Assuming a magnetic field distribution behaving as a potential function the mean magnetic field can be calculated. Additional ohmic losses appear due the electric current flow in the tube of short-cut core of the pump $P_{t,s}$ and the tube walls adjacent to the coils $P_t$. The current circulating in the tube walls $J_t$ can be estimated assuming ideal electrical contact at the fluid-wall interface using the relations:

$$J_t = \; (\lambda \cdot f)\; \sigma_t\, \overline{B}\; (\delta_t \cdot L)\; ; R_t = \frac{1}{\sigma_t} \cdot \frac{2}{\pi\, (d_a + \delta_t)}\; ;\; P_t = R_t \; \cdot \; J_t^2 \quad , \tag{33}$$

where $R_t$ is the wall resistance in Ohm ($\Omega$). Besides to the direct ohmic heating due to the current flow within the tube walls the ferromagnetic iron sheets within the core of the pump are also "*microwave*" heated. Although the iron sheets are separated from each other by a resistive oxide layer (which is electrically insulating) the electric currents induced into them can circulate throughout the inner core, because the sheets are embedded in the electrically conducting structural material. The appearing currents can hardly be calculated, but assuming an hyperbolic decay of the magnetic induction within the core the flux penetration can be assumed.

Finally, the current through the copper coils and the connection between the coils cause also an ohmic loss. The total resistance $R_{wind}$ in all coils as well as the power released there $P_{Coil}$ is then given by:

$$R_{wind} = \frac{4}{\pi} \frac{l_{coil}}{\sigma_{Cu}\, A_{coil}} \cdot n_{slots}; \quad P_{wind} = R_{Coil} \cdot I^2_{\sup ly} \quad , \tag{34}$$

where $A_{coil}$ is the current carrying cross section area of the winding, $l_{Coil}$ its length, $n_{slot}$ the amount of slots and $\sigma_{Cu}$ the specific conductivity of the copper.

The derived equations of section 2.2-2.6 are applied to two annular cylindrical induction pumps and the obtained calculated data are compared to the ones obtained by the model.

**3. Electro-Magnetic pumps considered for the model verification.** Within the **Mega**Watt **Pi**lot **E**xperiment (MEGAPIE) to be conducted at the **P**aul-**S**cherrer **I**nstitute (PSI) the feasibility of a lead-bismuth alloy cooled target for spallation purposes will be demonstrated. A major component of such targets are the pumps, which are necessary to remove the heat from the highly heat loaded window facing the proton beam generated by the accelerator and transporting the heat through the heat exchangers. A more detailed information about the MEGAPIE project may be taken from the internet.The Megapie target pump system is given by two pumps being arranged in series. One pump, the main pump, is providing a lead bismuth flow the so-called main flow towards an annular gap and a second pump is delivering the flow rate necessary for the cooling of the stagnation point in the center of the hemisphere of the beam window. In the present analysis we restrict our discussion on the main pump, operating with lead bismuth ($Pb^{45}B^{i45}$) in the temperature range 230 $^\circ$C-480 $^\circ$. Detailed information on the specific design may be taken from Dementjev et al. (2003) or Freibergs & Platacis (2002,2003).

The second pump type considered are annular linear induction pumps operating with sodium at temperatures from 120-500 $^\circ$C, which were used in the Karlsruhe dynamo experiment, see e.g. Müller and Stieglitz (1997, 2001, 2004)

The design parameters of the pumps considered are displayed in table 1. A principle sketch of both systems is shown in figure 2. The geometric dimensions of both pump units are given in table 2. The thermophysical data used in the calcualtions have been taken from Imbeni et. al (1999), Lyon (1952) and Yefimov et al. (1996).

From these geometrical values of the pump, the electric connection of the individual coils and the postulated pressure heads and flow rate one can derive the principle features of both pumps, which are given in table 3.

**4. Performance of the pumps and power balance.** Inserting the design parameters into the pump equation 25 and postulating the required flow rate and pressure head one obtains the electric current to be supplied by the coil windings to the duct as a function of the wavelength $\lambda$ at a given frequency $f$ of

*Table 1.* Design specification of the MEGAPIE pump and the dynamo pump.

| | Parameters | MEGAPIE- $Pb^{45}Bi^{55}$ | Dynamo Sodium |
|---|---|---|---|
| | $\Delta p$ [Pas $10^5$] | 0.2 | 3 |
| | flow rate $Q$ [$m^3$/h] | 18 | 130 |
| | electric Power [kW] | 8.2 | 51.34 |
| | active Power [kW] | 9.8 | 44.46 |
| | current $I[A]$ | 35 | 78 |
| | current density $j$ $[A/mm^2]$ | 6 | 2.786 |
| | potential $\phi$ $[V]$ | 108 | 380 |
| | phase shift $\varphi$g $\phi$,$I$ [$^\circ$] | 30 $^\circ$ | 30 $^\circ$ |
| | net frequency $f$[Hz] | 50 | 30 |
| | induction in Passive core $B[T]$ | 1.2 | 1.64 |
| | temperature $T_{op}[^\circ C]$ | 480 | 150 |

*Table 2.* Design parameters of Pb45Bi55 pump and sodium pump.

| | Design | MEGAPIE- $Pb^{45}Bi^{55}$ | Dynamo Sodium |
|---|---|---|---|
| | effective pump length $L$ [m] | 0.36 | 1.323 |
| | liquid metal gap $a$ [mm] | 15 | 8.5 |
| | inner diameter of flow channel $d_i$ [mm] | 102 | 121 |
| | outer diameter of flow channel $d_a$ [mm] | 122 | 138 |
| | mean diameter of flow channel $d_m$ [mm] | 107 | 129.5 |
| | wall thickness inductor $\delta_t$ [mm] | 1.5 | 3 |
| | wall thickness core $\delta_t$ [mm] | 1.5 | 2 |
| | air gap core inductor $\delta_{air}$ [mm] | 0.5 | 0.25 |

*Table 3.* Calculated induction features of both ALIP's.

| | design unit | relation | MEGAPIE | Dynamo |
|---|---|---|---|---|
| | wave length $\lambda$gmm] | $\lambda = L/n_{Pole}$ | 180 | 441 |
| | number of poles | | 3 | 3 |
| | mean fluid velocity $v_f$ [m/s] | $v_f = Q_{\max}/\mathrm{A_{Cross}}$ | 1.42 | 10.442 |
| | mean magnetic field velocity $v_B$ [m/s] | $v_B = \lambda \cdot f$ | 9 | 13.23 |
| | slip ratio s [/] | $s = (v_B - v_f)/v_B$ | 0.84211 | 0.21071 |
| | effective real efficiency $\eta$ [%] | $\eta = (1-s)\left(\frac{s}{1+s}\right)$ | 7.218 | 13.74 |

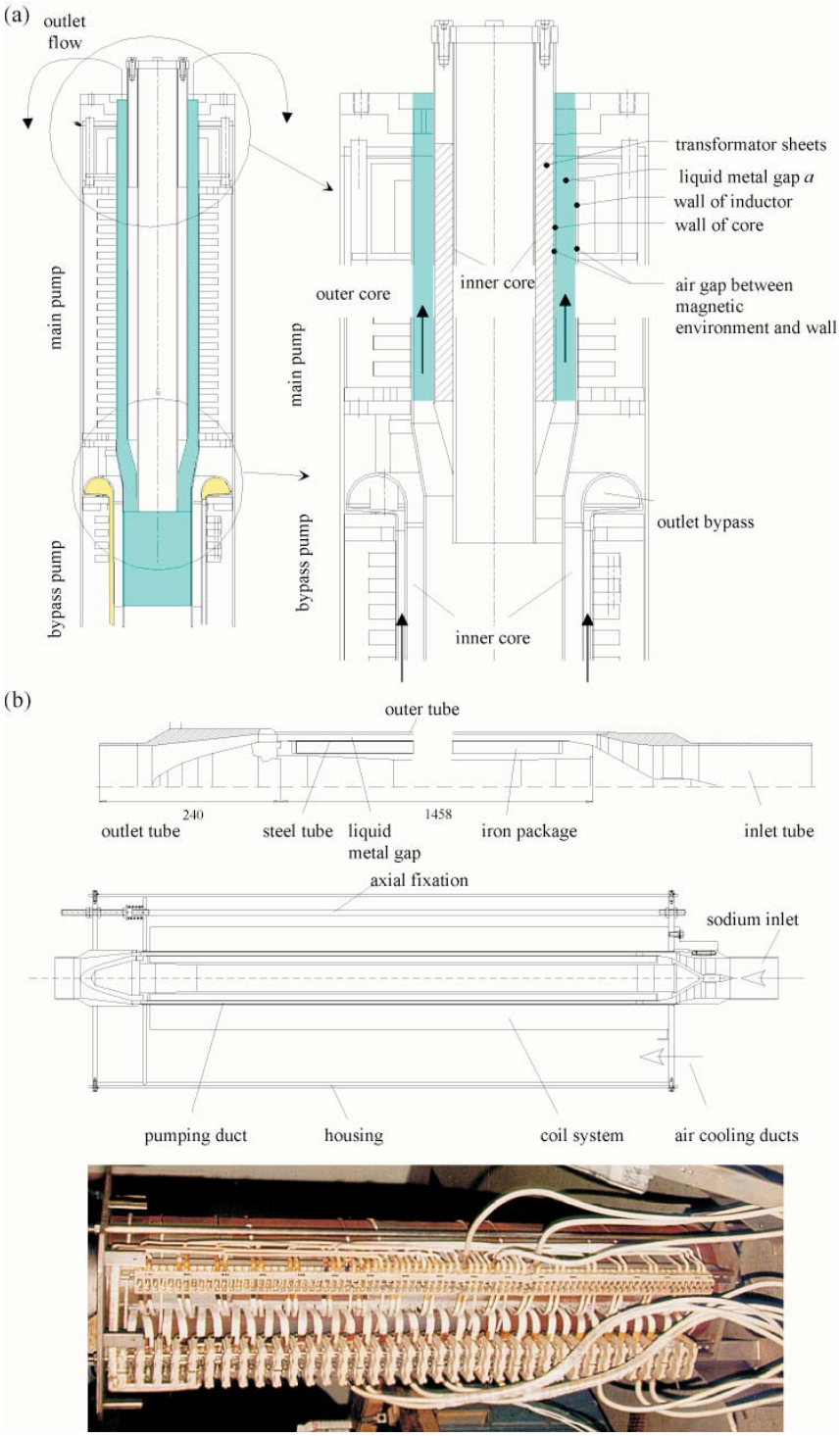


Fig. 2: (a) Principle sketch of the MEGAPIE main pump using Pb45BiBi55 Freibergs&Platacis (2002, 2003). (b) Schematic drawing and photograph of the inductor of the sodium pump used in the dynamo experiment, see Stieglitz & Müller (1997).

the travelling magnetic field. The figures 3 show the necessary current density per meter to be applied to the duct as a function of the wave length $\lambda$.

For the dynamo pump one obtains a local minimum of the current density for a wave length of $\lambda$=441mm and the related current density is *J=33051A/m*. The slip $s$ to be given by the design calculates to $s = 0.2107$, respectively. All these values hold for sodium at 150 $^\circ$C and have to be matched by the design. In case of the MEGAPIE pump the actual wave length is far away from the local minimum, which yields from the restricted space available for the desired operation.

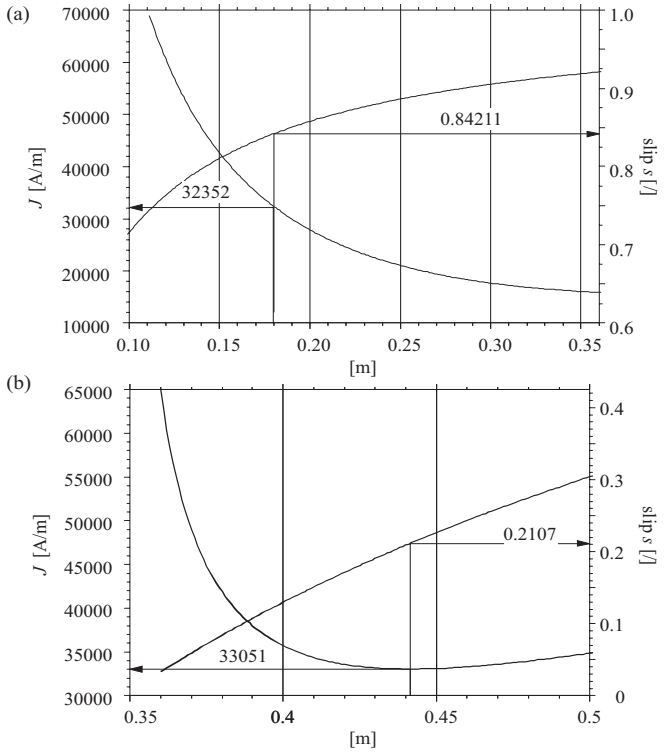


Fig. 3: Calculated required current supply to the duct and corresponding slip ratio as a function of the wave length $\lambda$ for the MEGAPIE pump (a) and the Dynamo (b).

In both pump designs MEGAPIE and the Dynamo the current carrying coils fill about 80% of the active length, while the ferro-magnetic iron sheets occupy the rest of domain. Applying the nominal operation current to the coil system in each of the pumps of the MEGAPIE units exhibits a real current density of 36360A/m is obtained, which is about 12% larger than the required current density per meter. In case of the dynamo pump a real current density of 45184A/m is obtained, which is considerably larger than the required one from fig. 3b.

For the calculation of the pump performance diagrams the dimensions of the slots and the winding set-up must be given,. Additionally, the connection between the coils is necessary. In case of the MEGAPIE pump all coils are interconnected in form of a triangle connection, whereas in the Dynamo pump a star triangle connection is used, which modifies eq.29a slightly. The detailed data may be taken from table 4.

Applying the nominal operation current to both pumps an idealized pressure flow rate diagram can be calculated. It does not account for the hydraulic losses

*Table 4.* Electric connection of the inductors of both ALIPS.

| | Design | MEGAPIE | Dynamo |
|---|---|---|---|
| | number of large slots per pole $n_{slots}$ | 9 | 6 |
| | number of small slots per pole $n_{slots}$ | - | 6 |
| | current turns per slot $n_{current,turns}$ | 24 | 27 |
| | number of poles $n_{Poles}$ | 2 | 3 |
| | slot width small $s_w$[mm] | - | 23.5 |
| | slot width large slot $s_w$[mm] | 11 | 36 |

in the piping and to the first order to the electro-magnetic end effects both at the inlet and outlet of the pump. If both effects are included according to the section 2.2-2.6 the flow rate pressure diagrams shown in the figures 4a, b describe the performance of both pumps.

The attainable pressure head especially at low flow rates (- small slip ratios-) is underestimated by the model for both pumps as shown in figures 4, because the model assumes that the magnetizing current is zero outside the pump, which is not true since the magnetic field there decays as potential field. Moreover, the ferro-magnetic parts are a little bit larger in both real configurations, so that the magnetic field smoothes out at both ends. A second effect leading to a smaller pressure calculated by the model is given by the assumption that the fluid velocity across the gap is considered as constant in order to keep the problem analytically tractable. This yields at lower slips, which appear at lower velocities to an overestimation of the ohmic losses and thus to a lower pressure. Besides all simplifications made the deviation between analytically calculated pressure head and experimentally found data is only about 5% in case of the Dynamo and there the deviations between model and experimental values decreases for increasing flow rates. Regarding the pump efficiency for the sodium a local efficiency maximum is obtained for a flow rate of approximately $90\mathrm{m}^3/\mathrm{h}$ which corresponds to a slip of almost 0.5. A further increase of the flow rate leads to higher pulsation losses and thus the efficiency decreases continuously beyond this point.

A similar situation is observed for the MEGAPIE application, where the calculated pressure is underestimated by the model at low slip ratios $s$. But here a deviation between model and experiment of about 10-15% remains also for the higher flow rates. One explanation for the deviation is that the slot width to active length ratio is not negligible which yields to strong pressure gradients $\mathrm{d}p/\mathrm{d}z$ along the pump. A second aspect for the deviation between the model and the experiment is related to the model assumption of a constant flow velocity in the pumping channel. If one calculates the pressure variation across the duct height in the MEGAPIE set-up a value of 1.67 is obtained, for which the previously made assumption of a constant flow velocity is for sure not valid.

Due to the high slip chosen in the design because of the limited length available in this application the efficiency is rather small and reaches only about 7% at the nominal operation point. Although it increases linearly with the flow rate it is considerably smaller than in the sodium case. One of the reasons for this behaviour is the weak specific electric conductivity of the eutectic PbBi alloy, which is even smaller than that of the stainless steel wall tubes. This yields to significantly larger current densities in the wall tubes of the PbBi application than in the sodium case, where the sodium is significantly better conducting than the wall tubes.

Fig. 4: Calculated (-—) pressure head of the MEGAPIE (a) and Dynamo (b) ALIP as a function of the flow rate at nominal current and the related pump

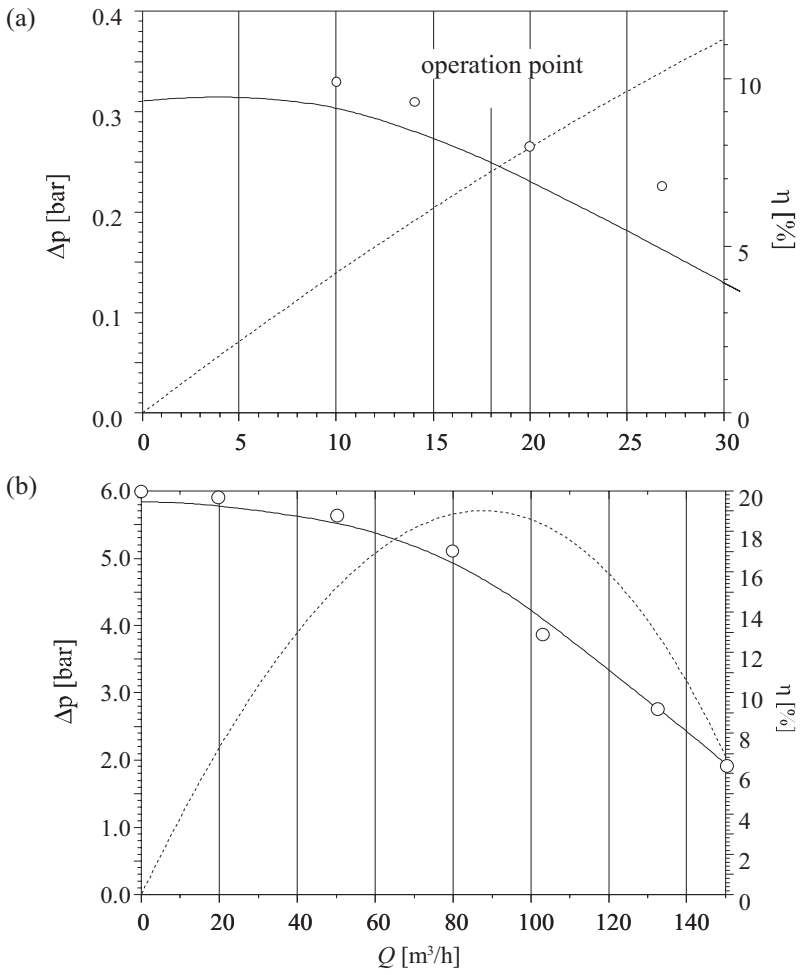
(a)
operation point
Δp [bar]
η [%]
0.0
0.1
0.2
0.3
0.4
0
5
10
15
20
25
30
(b)
Δp [bar]
η [%]
Q [m³/h]
0.0
1.0
2.0
3.0
4.0
5.0
6.0
0
20
40
60
80
100
120
140

efficiency $\eta$ in percent (- - -). The circles denote the measured pressure difference over the pump.

**5. Summary.** Within this article a simple two-dimensional model to calculate analytically linear induction pumps is derived. It contains the aspects of the losses due to end effects, the magnetic flux penetration in the pump, general design equations and some considerations about the power balance.

As an example for the applicability of the model two different existing annular linear induction pumps using two different liquid metals, namely sodium and the eutectic Lead-Bismuth alloy PbBi, have been chosen for the recalculation. For both of these pumps experimental data have been compared with the analytically calculated values.

The comparison of experimental and analytical data shows that the model underestimates the attainable pressure head in case of small slip ratios. This underestimation is based on an inadequate assumption for the magnetic induction outside the active length, which has been used to keep the solution analytical. But, at the small slip ratios the deviation is of order 10% so that it is acceptable. A second deficit of the model appears for large gaps of the duct channel, as appearing in case of the PbBi application for MEGAPIE. Large gap sizes yield to a strong pressure variation across the duct normal to the wall, which immediately lead to a non-uniform velocity profile. The assumed shape of the velocity profile, however, is an input to the model and has been set here to a constant value. Despite this inadequate velocity profile assumption the deviation between model and experiment does not increase too strong for larger flow rates. For the MEGAPIE application even 50% above the nominal operation the deviation between model and experiment does not exceed 20%.

*5.1. Acknowledgements* This work bas been performed in the context EU-program FIS5-2001-00090 MEGAPIE-TEST.

**References**

BEITZ, W, KÜTTNER, K.-H., 1986, Dubbel-Taschenbuch des Maschinenbaus, *Springer-Verlag,* $15^{th}$ edition; ISBN 3-540-12418-7, p. 1211 ff.

BLAKE, L.R., 1956, Conduction and induction pumps for liquid metals. The Institution of Electrical Engineers. *Unwin Brothers Limited Woking and London* UDC 621.313.1.621.88.

DEMENTJEV, S., GRÖSCHEL, F., IVANOV, S., PLATACIS, E., VON HOLZEN, G., ZIK, A., 2003, EMPS for MEGAPIE target. Testing of the Prototype. *PSI-Report MPR-11-DS34-005/0.*

FREIBERGS, E., PLATACIS, E. 2002, Electro-magnetic pump system- A detailed design. *Institute for Physics Report IPUL* 1069.00.00-05.

FREIBERGS, E., PLATACIS, E. 2003, EMP System for PbBi melt at 280 ° C-450 ° C- Long run test for EMPS Prototype. *Institute for Physics Report* $20^{th}$ Feb. 2003.

IMBENI, V. MARTINI, C., MASINI, S., PALOMBARINI, G., 1999, The properties of the eutectic alloys Pb55.5Bi and Pb17Li. *ENEA-Report DT-EUB-00001*, Part 2.

LYON, R.N. 1952 Liquid metals handbook; *Navexos P-733*; Second edition.

MÜLLER, U., STIEGLITZ, R., HORNAYI, S., 2004, A two-scale hydromagnetic dynamo experiment. *Journal Fluid Mechanics*,**498**, 31-72.

STIEGLITZ, R., MÜLLER, U. (1997) GEODYNAMO- An experimental facility to demonstrate the mean field dynamo-effect. *Proc.* $3^{rd}$*Int. Conf. on Energy Transfer in Magnetohydrodynamic Flows (PAMIR)*, $22^{nd}$-$26^{th}$Sept. 1997;Aussois-France; 1; p. 15-20.

STIEGLITZ, R, MÜLLER, U., 2001, Experimental demonstration of a homogeneous two-scale dynamo. *Physics of Fluids* **13**(3), 561-565.

STIEGLITZ, R., 2003, MHD Features of the main service and bypass pump in the MEGAPIE design. *FZKA Report 6826.*

YEFIMOV, E.I. 1996, Preconceptional design of a 1MW flow Lead-bismuth target. State Scientific Centre of Russian Federation- Institute of Physics and Power Engineering. *Report No. 35-06/64-1996.*